



AMERICAN METEOROLOGICAL SOCIETY

Journal of Physical Oceanography

EARLY ONLINE RELEASE

This is a preliminary PDF of the author-produced manuscript that has been peer-reviewed and accepted for publication. Since it is being posted so soon after acceptance, it has not yet been copyedited, formatted, or processed by AMS Publications. This preliminary version of the manuscript may be downloaded, distributed, and cited, but please be aware that there will be visual differences and possibly some content differences between this version and the final published version.

The DOI for this manuscript is doi:
10.1175/2009JPO4215.1

The final published version of this manuscript will replace the preliminary version at the above DOI once it is available.



An indicator of the multiple equilibria regime of the Atlantic Meridional Overturning Circulation

Selma E. Huisman, Matthijs den Toom and Henk A. Dijkstra¹,

Institute for Marine and Atmospheric Research Utrecht

Department of Physics and Astronomy, Utrecht University

Princetonplein 5, 3584 Utrecht, the Netherlands

and

Sybren Drijfhout

Royal Netherlands Meteorological Institute

De Bilt, the Netherlands

Revised for J. Phys. Oceanography

Version of October 4, 2009

¹Correspondence: Email: H.A.Dijkstra@uu.nl

Abstract

Recent model results have suggested that there may exist a scalar indicator Σ monitoring whether the Atlantic meridional overturning circulation (MOC) is in a multiple equilibrium regime or not. The quantity Σ is based on the net freshwater transport by the MOC into the Atlantic basin. It changes sign as soon as the steady Atlantic MOC enters the multiple equilibrium regime due to an increased freshwater input in the northern North Atlantic. This paper addresses the issue why the sign of Σ is such a good indicator for the multiple equilibrium regime. Changes in the Atlantic freshwater budget over a complete bifurcation diagram and in finite amplitude perturbation experiments are analyzed in a global ocean circulation model. We show that the net anomalous freshwater transport into/out of the Atlantic due to the interactions of the velocity perturbations and salinity background field is coupled to the background (steady-state) state freshwater budget and hence to Σ . The sign of Σ precisely shows whether this net anomalous freshwater transport is stabilizing or destabilizing the MOC. Therefore it can indicate whether the MOC is in a single or multiple equilibrium regime.

1 Introduction

Over the last decades serious concerns have been raised about possible anthropogenic induced changes in the ocean circulation and the consequences for climate (Rahmstorf, 2003). When the ocean velocity field is integrated in east-west direction across an ocean basin, the resulting flow is referred to as the meridional overturning circulation (MOC). In the Atlantic Ocean there is a net northward flow of surface and bottom waters, which is compensated for by a southward motion at intermediate depths. The Atlantic MOC transports a substantial amount (about 1.5 PW at 25°N) of heat northward. A reduction (collapse) of the MOC may therefore lead to serious climate change. Regions around the North Atlantic would experience significant cooling, and other parts of the world would also be affected (Vellinga *et al.*, 2002). Paleoclimate data suggests that such changes in the MOC may have occurred in the past (Clark *et al.*, 2002; Rahmstorf, 2002).

Although wind-generated motions influence the shallow part of the MOC, the deep overturning is dominantly driven by interior turbulent mixing of heat and salt, and is therefore referred to as the thermohaline circulation (THC). The spatial structure of the THC is predominantly determined by the ocean's density field (Wunsch, 2002; Kuhlbrodt *et al.*, 2007). Because the ocean flow itself influences the density field by advection, the THC is by implication a nonlinear phenomenon. Furthermore, the distribution and intensity of surface fluxes of heat and fresh water act to modulate the flow pattern and its temporal behavior.

The nonlinear nature of the THC may result in the existence of multiple equilibria (ME) for a given set of boundary conditions. Under present-day forcing conditions, two stable equilibria appear possible in models, one usually referred to as the 'on' state (or conveyor state) and the other as the 'off' state (or collapsed state). Traditionally large and abrupt changes in the Atlantic MOC have been related to the existence of multiple equilibria. These are a robust feature in models ranging from simple box ocean-only models (Stommel, 1961) to so-called EMIC's (Earth system

Models of Intermediate Complexity) (Rahmstorf *et al.*, 2005), and have also been found in early coupled climate models (Manabe and Stouffer, 1988). It is, however, not clear whether this is a common characteristic of state-of-the-art coupled (ocean-atmosphere) general circulation models (CGCMs) simulating present-day climate. In analyzing nine different CGCM simulations of the response to the IPCC SRES-A1B scenario of future CO₂ increase Schmittner *et al.* (2005), for example, found that none of these models predicted an abrupt change of the MOC.

As it is impossible at the moment to determine whether these CGCMs are in a multiple equilibrium regime, it is important to have (preferably scalar) indicators for the presence of such a regime. Using a simple box model, it was already pointed out by Rahmstorf (1996) that the multiple equilibrium regime may be related to the net freshwater budget over the Atlantic basin. This issue was revisited by De Vries and Weber (2005) who showed (using an EMIC) that the sign of the net freshwater export by the Atlantic MOC, indicated by $M_{ov}(\theta)$, near the latitude $\theta = 35^\circ\text{S}$ in the Atlantic may be controlling whether, in addition to the ‘on’ state, a stable ‘off’ state exists or not.

In Dijkstra (2007), it was shown that a measure of the divergence of the freshwater transport Σ of the Atlantic MOC over the Atlantic basin is a good indicator of the multiple equilibrium regime. When the freshwater transport at the northern boundary is neglected, Σ reduces to the indicator in De Vries and Weber (2005), since

$$\Sigma(\theta_n, \theta_s) = M_{ov}(\theta_s) - M_{ov}(\theta_n), \quad (1)$$

where θ_n and θ_s are the northern and southern latitudes of the Atlantic domain. It appears that Σ changes sign (from positive to negative) when the Atlantic MOC ‘on’ state enters the multiple equilibrium regime as the freshwater input in the northern North Atlantic is increased. There is a slight sensitivity to the choice of the southern boundary but $\theta_s = 35^\circ\text{S}$ appears a ‘best’ choice because the tip of Africa marks the southern boundary of the Atlantic basin. The sensitivity of Σ to

the northern latitude θ_n is relatively small as long as it is north of 60°N .

Although the indicator Σ seems to be able to serve as an indicator for the multiple equilibria regime and descriptive explanations were given in De Vries and Weber (2005) and Dijkstra (2007), there is a need for a better physical basis of this indicator which can explain why Σ crosses zero when entering the multiple equilibrium regime and why the southern boundary 35°S is so important. The main purpose of this paper is to provide strong support that Σ is a correct indicator for distinguishing different MOC regimes.

The advantage of the approach and methodology followed in Dijkstra (2007) is that full bifurcation diagrams are available and that steady states on the ‘on’ and ‘off’ branches satisfy integrated (freshwater) balances with a relative error smaller than 0.1%. In particular, the availability of the unstable steady state — which was shown in Dijkstra *et al.* (2004) to separate the regions (the so-called attraction basins) of initial conditions going to either ‘on’ and ‘off’ states — enables targeted studies on the development of finite amplitude perturbations.

To be self-contained here, we start in section 2 below with a very brief summary of the main results in Dijkstra (2007). In section 3, we analyze details of the Atlantic freshwater balance and provide a physical description of the processes that are involved in the changes of this balance along a full bifurcation diagram. In section 4, the transient development of specific finite amplitude perturbations is studied with focus on the processes determining MOC recovery and collapse. The analyses in the sections 3 and 4 provide a physical explanation why the sign of Σ is a good indicator for the multiple equilibrium regime. The results are summarized and discussed in section 5. Here we also address the usefulness of Σ in CGCMs and observations and whether it is, in principle, possible to use the indicator to assess the stability regime of the present-day MOC.

2 The indicator Σ in a global ocean model

Bifurcation diagrams were computed in Dijkstra (2007) using a fully-implicit global ocean model. Just to stress that this is no ‘toy’ model, we mention that the governing equations of this ocean model are the hydrostatic, primitive equations in spherical coordinates on a global domain which includes full continental geometry as well as bottom topography (Dijkstra and Weijer, 2005). Horizontal and vertical mixing of momentum and heat/salt is represented by a Laplacian formulation with prescribed constant ‘eddy’ viscosities A_H and A_V and vertically dependent ‘eddy’ diffusivities $K_H(z)$ and $K_V(z)$ Dijkstra (2007). The ocean flow is forced by the annual-mean wind stress as given in Trenberth *et al.* (1989). The upper ocean is coupled to a simple energy-balance atmospheric model (see the Appendix in Dijkstra and Weijer (2005)) in which only the heat transport is modelled (no moisture transport). The freshwater flux is prescribed and the model has no sea-ice component.

Starting from the steady state solution determined under restoring conditions for the surface salinity field (Levitus, 1994), steady states were calculated in Dijkstra (2007) versus a parameter γ_p under the freshwater flux $F_S = P - E$ with

$$F_S = F_S^e + \gamma_p F_S^p - Q, \quad (2)$$

where F_S^p is unity only in the domain $(\phi, \theta) \in [60^\circ W, 24^\circ W] \times [54^\circ N, 66^\circ N]$ and zero outside. Furthermore, F_S^e is freshwater flux diagnosed from the solution at $\gamma_p = 0$. The quantity Q is determined such that

$$\int_{S_{oa}} F_S r_0^2 \cos \theta \, d\theta d\phi = 0, \quad (3)$$

where S_{oa} is the total ocean surface and r_0 is the radius of the Earth, to ensure a net zero freshwater flux over the total ocean surface.

For the case that the vertical diffusivity K_V increases from $1.2 \times 10^{-4} \text{ m}^2\text{s}^{-1}$ at the surface to $5.3 \times 10^{-4} \text{ m}^2\text{s}^{-1}$ near the bottom of the flow domain, the bifurcation diagram, where the maximum of the Atlantic MOC (ψ_A) is plotted versus γ_p , is

shown in Fig. 1a. For clarity, the stable (drawn) branches are indicated with the ‘on’ branch and with the ‘off’ branch. The dashed branch represents unstable steady states. It is clear that the saddle-node bifurcations L_- and L_+ limit the multiple equilibria regime; we indicate the values of γ_p at these points with γ_{L-} and γ_{L+} , respectively.

Solutions of the Atlantic MOC along several labeled points of the bifurcation diagram in Fig. 1a are plotted in Fig. 2a-f. For small γ_p , the solution of the Atlantic MOC (the ‘on’ state) is near to the unperturbed state with strong northern sinking and no bottom water of southern origin (Fig. 2a). Along the bifurcation diagram, the strength of the Atlantic MOC decreases (Fig. 2b) with increasing γ_p until the saddle-node bifurcation at γ_{L+} . In the pattern of the Atlantic MOC, the return flow shallows (Fig. 2c) and the deep flow from the south strengthens. Once on the unstable branch of steady states from L_+ to L_- , this southern sinking component increases leading eventually to the stable ‘off’ state (Fig. 2d-f) for values of $\gamma_p > \gamma_{L-}$ on the lower (drawn) branch in Fig. 1. For values of γ_p between γ_{L-} and γ_{L+} , the MOC is in the multiple equilibrium (ME) regime. For $\gamma_p < \gamma_{L-}$ and $\gamma_p > \gamma_{L+}$ only one stable steady state exists, and the MOC is in the single equilibrium (SE) regime.

The indicator Σ in Dijkstra (2007) is based on the freshwater budget which arises when the stationary salinity equation is integrated over a volume V of the Atlantic Ocean bounded by the latitudes θ_s and θ_n . This integrated salinity budget can be written as

$$\int_{S_{Atl}} F_S r_0^2 \cos \theta \, d\phi d\theta = -\frac{1}{S_0} (\Phi(\theta_n) - \Phi(\theta_s)). \quad (4)$$

In (4), the left hand side is the freshwater volume (in Sv) going through the ocean-atmosphere surface S_{Atl} and the right hand side is the net freshwater transport (in Sv) through the lateral boundaries at θ_n and θ_s . The salt flux Φ is defined as

$$\Phi(\theta) = \int_{S_\theta} \left(vS - \frac{K_H}{r_0} \frac{\partial S}{\partial \theta} \right) r_0 \cos \theta \, d\phi dz, \quad (5)$$

where S_θ is the (zonal-vertical) ocean section at latitude θ .

The indicator $\Sigma(\theta_s, \theta_n)$ was already given in (1) where, following De Vries and Weber (2005), M_{ov} (the overturning component) and M_{az} (the azonal component) are defined as

$$M_{ov}(\theta) = -\frac{\eta}{S_0} \int \langle v \rangle (\langle S \rangle - S_0) dz ; M_{az}(\theta) = -\frac{\eta}{S_0} \int \langle v' S' \rangle dz. \quad (6)$$

Here, η and $\langle F \rangle$ (for a function F) are given through

$$\eta = \int r_0 \cos \theta d\phi ; \langle F \rangle = \frac{1}{\eta} \int F r_0 \cos \theta d\phi \quad (7)$$

with $v' = v - \langle v \rangle$ and $S' = S - \langle S \rangle$. The indicator $\Sigma(\theta_s, \theta_n)$ is plotted along the ‘on’-branch of Fig. 1a in Fig. 1b for $\theta_n = 60^\circ\text{N}$ (in the sinking region) and $\theta_s = 35^\circ\text{S}$ (at the southern tip of Africa). Σ changes sign (from positive to negative) just as the multiple equilibrium regime is approached (near the saddle-node bifurcation L_-). In the SE regime, the Atlantic MOC exports salt ($\Sigma(\theta_s, \theta_n) > 0$) while in the ME regime, it is exporting freshwater ($\Sigma(\theta_s, \theta_n) < 0$).

It is remarkable that the indicator Σ , which is evaluated on the ‘on’ branch, is able to detect the presence of the saddle-node bifurcation L_- which is located on the ‘off’ branch. Certainly, the ‘on’ states for $\gamma_p > \gamma_{L_-}$ are linearly stable (i.e., very small perturbations on these states will decay), but they are susceptible to finite amplitude instabilities. As was shown in Dijkstra *et al.* (2004), the attraction domains of the ‘on’ state and ‘off’ state seem to be bounded by the unstable state and so it requires a finite amplitude perturbation which crosses the unstable branch to make a transition from the ‘on’ state to the ‘off’ state. But how would Σ provide any information on the presence of the multiple equilibrium regime and hence on the behavior of finite amplitude perturbations? In the next sections, we will investigate this systematically by analyzing details in the freshwater balances along both the ‘on’ and ‘off’ branches (section 3) and by considering the transient development of finite amplitude disturbances on the ‘on’ state (section 4).

3 Freshwater balance of the equilibria

When we represent the diffusive fluxes as

$$M_d(\theta) = \int_{S_\theta} \frac{K_H}{r_0} \frac{\partial S}{\partial \theta} r_0 \cos \theta \, d\phi dz, \quad (8)$$

and use the notation

$$M_{E-P} = \int_{S_{Atl}} S_0(E - P) r_0^2 \cos \theta \, d\phi d\theta, \quad (9)$$

the total freshwater balance (4) can be written as

$$M_{az}(\theta_n) + M_{ov}(\theta_n) + M_d(\theta_n) - M_{az}(\theta_s) - M_{ov}(\theta_s) - M_d(\theta_s) + M_{E-P} = 0 \quad (10)$$

The terms in this equation are shown in Fig. 3a (southern boundary) and Fig. 3b (northern boundary). As was shown in Dijkstra (2007), the freshwater balance (10) is satisfied accurately in this model. We see that the terms at the northern boundary (Fig. 3a) are smaller than the corresponding terms at the southern boundary (Fig. 3b), that the diffusive terms are not small with respect to the other terms and that many parts of the curves are characterized by near straight lines. In the subsections 3.1 and 3.2 below we study the latitudinal dependence of M_{ov} and M_{az} on the ‘off’ and ‘on’ branches and the change of $M_{ov}(\theta_s)$ along the ‘on’ branch.

3.1 Behavior of M_{ov} and M_{az} on the ‘off’ branch

The function $M_{az}(\theta)$ is plotted in Fig. 4a. The azonal transport south of $\theta = 10^\circ\text{S}$ is driven by the subtropical gyre in the South Atlantic, with southward (northward) flow in the western (eastern) part of the basin. The salinity field S' (not shown) at the ‘off’ solution in Fig. 2f for $\theta_s = 35^\circ\text{S}$ is negative in the western part of the basin and positive in the eastern part, the value of M_{az} is negative and the gyres transport freshwater out of the basin. With decreasing γ_p , the salinity field S' changes to become more positive at the western side of the basin and more negative at the eastern part. Hence the value of M_{az} becomes less negative. The changes in S'

go down to about 1000 m while in deeper levels S' is hardly affected by the addition of salt in the northern North Atlantic. It is interesting that M_{az} becomes zero near $\theta = 35^\circ\text{S}$ at the saddle-node bifurcation L_- (very close to the solution in Fig. 2d). This indicates that the saddle-node bifurcation, which is a signal of ‘nonexistence’ of a steady solution, is connected to the gyre driven freshwater transport over the southern boundary.

The function $M_{ov}(\theta)$ is plotted in Fig. 4b and shows that the ‘off’ state Atlantic MOC is exporting salt south of 10°S . For the solution in Fig. 2f, $\langle v \rangle$ is strongly negative in the upper ocean and the mean salinity $\langle S \rangle - S_0 > 0$ which leads to a positive $M_{ov}(\theta)$. When γ_p decreases (effectively adding salt in the northern North Atlantic), the mean salinity at 35°S increases over the whole depth and the mean surface velocity decreases slightly, leading to a slight increase in $M_{ov}(\theta)$ at $\theta = 35^\circ\text{S}$ (Fig. 4b).

3.2 Behavior of M_{ov} and M_{az} on the ‘on’ branch

The latitudinal dependence of M_{az} is plotted in Fig. 5a for the solutions in Fig. 2a-c. South of $\theta = 20^\circ\text{S}$, the gyre driven freshwater transport is positive, i.e. the gyres transport salt into the basin. Again the velocity distributions v' are fairly similar to those along the ‘off’ branch (because the winds are the same), but now the salinity distributions S' are quite different with positive values in the western part of the basin and negative ones at the eastern part of the basin. With increasing γ_p (adding freshwater in the northern North Atlantic), the fields S' hardly change and hence M_{az} south of 20°S remains constant with γ_p . The reason is that the freshwater anomaly is transported southward at depth by the ‘on’ state and therefore this does not affect the azonal transport.

In Fig. 5b the function $M_{ov}(\theta)$ is positive at the solution in Fig. 2a south the equator as the ocean velocity at depth $\langle v \rangle$ is negative where the salinity $\langle S \rangle$ is largest. Hence the meridional overturning transports salt out of the basin. When

γ_p is increased, one sees the decrease in mean salinity at depth while the salinity at the surface increases. This implies that M_{ov} must decrease with increasing γ_p as is seen in Fig. 2a.

Actually, it appears that there is linear behavior of M_{ov} with γ_p on the ‘on’ branch due to the specific choice of the forcing. When we differentiate the forcing (2) to γ_p , we find that it is a positive constant, say $\alpha > 0$, and hence

$$M_{E-P} = M_{E-P}^0 - \alpha\gamma_p \quad (11)$$

Here, the superscript in M_{E-P}^0 indicates the solution for $\gamma_p = 0$, i.e., the reference solution. The linear relation in (11) is clearly seen in Fig. 3.

Using the notation $\Sigma_{az} = M_{az}(\theta_s) - M_{az}(\theta_n)$ and $\Sigma_d = M_d(\theta_s) - M_d(\theta_n)$, we can write the equation (10) as

$$\Sigma + \Sigma_{az} + \Sigma_d = M_{E-P}. \quad (12)$$

We argued above that Σ_{az} does not change much along the ‘on’ branch and it appears from Fig. 3 that the same holds for Σ_d . Using this result, (11) and the fact that $M_{E-P}^0 = \Sigma^0 + \Sigma_{az}^0 + \Sigma_d^0$ for the reference solution, we find that

$$\Sigma \approx -\alpha\gamma_p + \Sigma^0. \quad (13)$$

This indicates that Σ has a zero on the ‘on’ branch with increasing γ_p (as $\alpha > 0$) when $\Sigma^0/\alpha < \gamma_{L+}$. Physically this simply means that the input of freshwater in the northern North Atlantic eventually leads to export of freshwater by the Atlantic meridional overturning circulation.

Although from (13) it is clear that Σ decreases along the ‘on’ branch, it is not at all guaranteed that it is changing sign near γ_{L-} . The question is therefore: why are the sign changes of the quantities Σ and the zonal salinity difference on the ‘on’ branch associated with the existence/non-existence boundary of the ‘off’ branch? This is a highly nonlinear problem as the issue is whether a finite amplitude perturbation to the ‘on’ state is able to recover or not. In the unique regime, one

can put any perturbation on the MOC but it will always recover. In the multiple equilibrium regime there always exists a finite amplitude perturbation which is able (i.e., which is large enough) to induce a transition to the (stable) ‘off’ state for the same value of γ_p . Hence, an analysis of the development of finite amplitude perturbations in both regimes is required and this is the focus of the next section.

4 Development of finite amplitude perturbations

In this section, we investigate why the ‘on’ state of the MOC always recovers in the SE regime but that in the ME regime the ‘off’ state can be reached. Thereto we apply specific finite amplitude freshwater perturbations by considering the so-called thermohaline pulse response problem (similar to the approach in Dijkstra *et al.* (2004)), where the freshwater perturbation is switched on instantly and after a certain time (t_m) is suddenly reduced to zero. If we represent the time dependence as a block function $B(t; t_m)$, then the total freshwater flux can be written as

$$F_S = F_S^e + (\bar{\gamma}_p + \Delta\gamma_p B(t; t_m)) F_S^p - Q(t) \quad (14a)$$

$$B(t; t_m) = H(t) - H(t - t_m) \quad (14b)$$

where H is the Heaviside function and $Q(t)$ is determined from the condition that the surface integrated freshwater flux is zero. The value of $\bar{\gamma}_p$ refers to the value of γ_p at a steady state and we use $\Delta\gamma_p$ as a perturbation of it. To facilitate the interpretation of the results, we choose to make the pattern of the freshwater perturbation associated with $\Delta\gamma_p$ the same as that for which the bifurcation diagram (in γ_p) was computed.

4.1 Transient solutions

Now let us assume we start from a steady state solution determined for a certain $\bar{\gamma}_p$ on the ‘on’ branch. When $\Delta\gamma_p = 0$, we will remain at that steady state. However, when $\Delta\gamma_p$ is so large that

$$\gamma_p = \bar{\gamma}_p + \Delta\gamma_p > \gamma_{L+} \quad (15)$$

the solution will be attracted to the ‘off’ state for $\bar{\gamma}_p + \Delta\gamma_p$ since this is the only steady state for this value of γ_p . After a time t_m , the trajectory will reach a certain state and when the anomalous forcing is then suddenly released, the trajectory will be attracted to one of the stable steady states which are present for $\gamma_p = \bar{\gamma}_p$. In the SE regime, there is only one steady state at $\bar{\gamma}_p$ and all trajectories (for all values of t_m) will be attracted to the ‘on’ state; hence the MOC always recovers. In the ME regime, however, the MOC will recover for small t_m while the ‘off’ state will be reached for large t_m . In Dijkstra *et al.* (2004) it was shown that the critical time, say t_m^* , is determined by the time when the unstable steady state is crossed.

We take a value $\bar{\gamma}_p^S = 0.083$ Sv in the SE regime and a value $\bar{\gamma}_p^M = 0.166$ Sv in the ME regime. Plots of the meridional velocity field and salinity field at 35°S are presented in Fig. 6 for both steady states. The meridional velocity fields look very similar for both cases although the MOC is slightly shallower in Fig. 6c than in Fig. 6a. The salinity fields differ markedly with a much larger salinity contrast between surface and deep ocean in the ME regime. This reflects the change in freshwater transport by the MOC over this section which is positive (freshwater transport into the Atlantic basin) in the SE regime and negative (freshwater transport out of the basin) in the ME regime.

To analyze the development for relatively small $\Delta\gamma_p$, we show results for both cases when the states in Fig. 6 undergo a change of $\Delta\gamma_p^S = \Delta\gamma_p^M = 0.02$ Sv for $t_m = 200$ year. The maximum of the Atlantic MOC (ψ_A) is plotted versus time in Fig. 7a and the drawn curves (red, SE regime; blue, ME regime) show the long time development under this change in freshwater flux. After about 200 years, the MOC strength has decreased less than 1 Sv for both cases. When the anomalous forcing is released at $t_m = 20$ and $t_m = 100$ yr (dashed curves), the original equilibria are obtained showing that the steady states are indeed linearly stable.

Subsequently, we take $\Delta\gamma_p^S = 0.197$ Sv and $\Delta\gamma_p^M = 0.114$ Sv, respectively such that for $t_m \rightarrow \infty$ the same ‘off’ state at $\gamma_p = 0.280$ Sv is reached (cf. Fig. 1). This is

confirmed by the drawn curves in Fig. 7b. The dashed curves in Fig. 7b again show the development of the MOC strength when the anomalous forcing is turned to zero (i.e., $\gamma_p = \bar{\gamma}_p$) after a time t_m . It is indeed seen that for every t_m the trajectories in the SE regime (red curves) eventually end up on the ‘on’ state. However, for the ME regime (blue curves) we see that for $t_m < t_m^*$, the Atlantic MOC recovers but that for $t_m > t_m^*$, the Atlantic MOC approaches the ‘off’ state; here the critical time $t_m^* \approx 400$ yr.

4.2 Analysis

We now turn to a physical explanation of the results in Fig. 7. Our task is to explain why (i) the MOC recovers in the ME regime for $t_m < t_m^*$, and collapses for $t_m > t_m^*$ and (ii) explain why the MOC in the SE regime, when subjected to a similar perturbation, always recovers. Our ingredients are that $\Sigma \approx M_{ov}(\theta_s) < 0$ for the steady ‘on’ state in the ME regime and $\Sigma \approx M_{ov}(\theta_s) > 0$ in the SE regime.

The existence of multiple equilibria in the MOC is caused by the salt advection feedback, which is present in its simplest form in the Stommel (1961) box model. A freshwater perturbation on the ‘on’ state of the MOC, for example, causes a weakening of the MOC and hence leads to a smaller meridional advective salt transport which amplifies the original perturbation. As advective meridional transport is crucial, this feedback has also been identified in two- and three dimensional ocean models (Walín, 1985; Dijkstra and Molemaker, 1997; Kuhlbrodt *et al.*, 2007).

If a perturbation (\tilde{v}, \tilde{S}) is assumed on a mean state (\bar{v}, \bar{S}) , the development of the salinity perturbation is determined (considering only meridional advective transport and hence neglecting all other (zonal/vertical advection and diffusive) transports) by the equation

$$\frac{\partial \tilde{S}}{\partial t} \approx -\frac{1}{r_0} \left[\tilde{v} \frac{\partial \bar{S}}{\partial \theta} + \bar{v} \frac{\partial \tilde{S}}{\partial \theta} + \tilde{v} \frac{\partial \tilde{S}}{\partial \theta} \right]. \quad (16)$$

When we integrate (16) over the Atlantic basin (longitude ϕ from coast to coast, z from bottom to surface and latitude θ from θ_n to θ_s), then the development of the

Atlantic basin averaged salinity anomaly is governed by the equation

$$\frac{\partial}{\partial t} \left(\int_V \tilde{S} d^3x \right) \approx \int_{S_{\theta_s}} (\tilde{v}\bar{S} + \tilde{S}\bar{v} + \tilde{v}\tilde{S}) d^2x \quad (17)$$

where the fluxes through the northern boundary are neglected. This relation shows that the growth of the salinity anomaly in the Atlantic basin is related to the anomalous meridional salt transport terms integrated over the southern boundary.

In the following, we will investigate the time development of the different terms in the right hand side of (17) along the trajectories in Fig. 7a. We will call the contribution of a certain term in the (17) ‘stabilizing’ (‘destabilizing’) when it increases (decreases) the salt content of the Atlantic basin and hence strengthens (weakens) the MOC. The terms are plotted in Fig. 8a for $\Delta\gamma_p = 0.02$ Sv. Note that because this value of $\Delta\gamma_p$ is relatively small, both linear interaction terms are of larger magnitude than the nonlinear interaction term $\tilde{v}\tilde{S}$. The $\bar{v}\tilde{S}$ term is positive for both SE and ME regimes and this transport is stabilizing the MOC. The nonlinear interaction term is negative (making the Atlantic fresher) and hence is destabilizing the MOC for both regimes. The central result is that the $\tilde{v}\bar{S}$ term is stabilizing in the SE regime, while it is destabilizing for the ME regime.

To understand the sign of the terms in (17), plots of \tilde{v} and \tilde{S} are shown in Fig. 9 for the solutions at year 200 (endpoints of drawn curves in Fig. 7a). For both ME and SE regimes, the \tilde{S} field is positive at the surface and negative at depth, which is a typical response to the slowdown of the MOC. As the \bar{v} term is largest at the surface (cf. Fig. 6a), the anomalous salt transport associated with the term $\bar{v}\tilde{S}$ is into the basin and hence is stabilizing. As \tilde{v} is negative at the surface and positive at depth (Fig. 9a,c), the nonlinear interaction term $\tilde{v}\tilde{S}$ always leads to salt export out of the Atlantic basin and hence this term is destabilizing.

The $\tilde{v}\bar{S}$ field is plotted for the SE and ME regimes (again at year 200) in the Figs. 10a,b, respectively and their difference is shown in Fig. 10c. The change in steady state salinity field with γ_p turns out to be crucial for the sign of the $\tilde{v}\bar{S}$ term. The salinity \bar{S} is smaller in the deep ocean (below ~ 3 km) for the solution in the

ME regime than for the SE regime. Hence the transport of salt due to the $\tilde{v}\bar{S}$ term is out of the Atlantic basin in the ME regime and into the Atlantic basin for the SE regime. Hence, this term is stabilizing in the SE regime and destabilizing in the ME regime.

We can make the link of the section integral over $\tilde{v}\bar{S}$ and $M_{ov}(\theta_s)$ more explicit by looking at the relation between the profiles of $\langle\bar{v}\rangle$ (Fig. 11a) and $\langle\tilde{v}\rangle$ (plotted for different times in Fig. 11b). By inspection, it appears that for both regimes, it is a reasonable assumption that $\langle\tilde{v}\rangle \approx -\epsilon(t)\langle\bar{v}\rangle$. Physically, this makes sense because the MOC decreases due to the imposed change in freshwater flux in the northern North Atlantic and the overall spatial pattern of the MOC remains the same for small $\Delta\gamma_p$. In other words, there is a southward velocity perturbation in the upper layers and a northward velocity perturbation at depth.

When we now decompose $\tilde{v} = \langle\tilde{v}\rangle + \tilde{v}'$, $\bar{S} = \langle\bar{S}\rangle + \bar{S}'$, then the section integral can be written as

$$\int_z \int_\phi \tilde{v}\bar{S} r_0 \cos\theta d\phi dz = \eta \int_z \langle\tilde{v}\rangle\langle\bar{S}\rangle dz + \int_z \int_\phi \tilde{v}'\bar{S}' r_0 \cos\theta d\phi dz \quad (18)$$

Using $\langle\tilde{v}\rangle \approx -\epsilon(t)\langle\bar{v}\rangle$, the first term in the right hand side is proportional to $M_{ov}(\theta_s)$. The second integral is dependent on the azonal components of \tilde{v} and \bar{S} . For both SE and ME cases in Fig. 8a, the three integrals in (18) are plotted in Fig. 8b. For the ME-regime (blue curves) the integral involving the $\tilde{v}'\bar{S}'$ term is much smaller than that involving the $\langle\tilde{v}\rangle\langle\bar{S}\rangle$ term. Hence, the sign of the section integral of $\tilde{v}\bar{S}$ is the same as that of M_{ov} at 35°S. For the SE case the integrals in the right hand side of (18) are of the same order of magnitude, so here the relation between the sign of the $\tilde{v}\bar{S}$ integral and M_{ov} at 35°S is less obvious. However, from Fig. 8b, it is clear that the sign of the $\tilde{v}\bar{S}$ term is most influenced by the changes in sign of the $\langle\tilde{v}\rangle\langle\bar{S}\rangle$ term.

From Fig. 8a, it can furthermore be seen that the stabilizing term $\bar{v}\bar{S}$ decreases and the destabilizing term $\tilde{v}\bar{S}$ becomes more negative (more destabilizing) with increasing γ_p . This demonstrates that when the ‘on-state’ of the MOC enters the

ME regime, the salt transport near the southern boundary induced by changes in the northern North Atlantic freshwater flux tend to be more destabilizing. In the analysis above, the salt transport at the northern boundary θ_n is assumed to be much smaller than that at the southern boundary θ_s , but it can easily be taken into account in (17). Following (18), the integral of the term $\tilde{v}\bar{S}$ over the northern and southern boundary can then be related to Σ . Hence, assuming a dominance of the meridional advective transport terms, the sign change in the $\tilde{v}\bar{S}$ term, as directly linked to Σ , is the crucial effect determining whether the MOC is in the SE or ME regime. When the perturbations become very large, as in the results of Fig. 7b, the pattern of the MOC changes drastically with time. Eventually, the magnitudes of all terms in (17) along the drawn trajectories in Fig. 7b will determine whether the MOC will collapse or recover when the forcing is released.

4.3 Further analysis in a box model

To substantiate the reasoning in the last subsection, we analyze the same connection between properties of the steady states and the transient development of perturbations in the Rahmstorf (1996) model. In this box model, only the meridional advective processes are taken into account. The model consists of two equatorial boxes connected to two polar boxes that are arranged as depicted in Fig. 12a. It is designed to mimic the pattern of the Atlantic circulation, with deep convection at subpolar latitudes (box 2), while low-latitude upwelling is limited (hence no connection between boxes 3 and 4), but instead takes place outside the domain of the Atlantic (box 1). The volume transport between the boxes has strength m and is proportional to the density difference $\rho_2 - \rho_1$. Assuming a linear equation of state, the flow strength is diagnosed from

$$m = k(\rho_2 - \rho_1) = k[\beta(S_2 - S_1) - \alpha(T_2 - T_1)], \quad (19)$$

where k , β and α are constants and T_i and S_i are the temperature and salinity in box i .

Mixed boundary conditions are imposed, where temperatures will be simply prescribed and the surface freshwater forcing consists of two independent active fluxes, F_1 and F_2 . The adjective ‘active’ here means that not only atmospheric vapor fluxes are captured in the F_i , but also the salt transport by the wind-driven gyres as well as (sub-grid scale) diffusion. The fluxes F_i are converted to equivalent salt transports by multiplication with $-S_0$, a fixed reference salinity, and will be assumed constant. The salt conservation equation for the southern box is then given by

$$V_1 \frac{dS_1}{dt} = \left\langle \begin{array}{c} m(S_4 - S_1) \\ m(S_1 - S_3) \end{array} \right\rangle + S_0 F_1 \quad \text{for} \quad \begin{array}{l} m \geq 0. \\ m \leq 0. \end{array} \quad (20)$$

Here, V_1 is the fixed volume of box 1. The equations for the other boxes follow in a similar fashion (Rahmstorf, 1996).

For $m \geq 0$, the steady state salinity in box 2 is equal to that in box 4, $\bar{S}_2 = \bar{S}_4$. Combination of equations (19) and (20) then yields the steady-state flow strength as function of the temperature contrast and the freshwater forcing:

$$\bar{m} = -\frac{1}{2}k\alpha(T_2 - T_1) \pm \sqrt{\frac{1}{4}[k\alpha(T_2 - T_1)]^2 - k\beta S_0 F_1} \quad \text{for} \quad \bar{m} \geq 0. \quad (21)$$

For $\bar{m} \leq 0$, the solution is similar to (21), but with $-F_1$ replaced by $+F_2$.

We will only consider the case for which $T_1 > T_2$. For $\bar{m} \geq 0$ solutions exist for $F_1 \in (-\infty, F_1^{Crit})$, where $F_1^{Crit} = k\alpha^2(T_2 - T_1)^2/4\beta S_0$, the critical freshwater flux at the saddle-node bifurcation. We are primarily interested in the transition associated with the sign change of F_1 , which Rahmstorf (1996) identified with the transition from the single equilibrium to the multiple equilibrium regime. The bifurcation diagram for this case is plotted in Fig. 12b, showing all steady solutions for $\bar{m} \geq 0$. Note that for $\bar{m} \leq 0$ solutions exist for $F_2 \geq 0$, independent of F_1 . However, this inverse circulation implies that all upwelling takes place in the northern box, despite the absence of a physical mechanism to limit dominant upward motion to the northern high latitudes. Hence, the applicability of the box model ends when

the flow reverses sign. For simplicity we define any situation for which $\bar{m} < 0$ as the collapsed state and we take $F_2 > 0$ to ensure that the trajectories are attracted to this state when m becomes negative.

Suppose we perturb the equilibrium given by equation (21) by applying an anomalous freshwater flux of strength γ_p to box 2 for a time t_m . Simultaneously an equal amount of water is extracted from boxes 1 and 3, in a ratio defined by their respective surface areas A_1 and A_3 , in order to preserve salinity. This will change the salinity contrast between boxes 1 and 2 such that the flow is weakened, but γ_p and t_m are chosen such that m does not reverse sign during the application of the perturbation. In the first two experiments F_1 is taken slightly negative ($F_1 = -10^{-3}$ Sv), and in the latter two slightly positive ($F_1 = 10^{-3}$ Sv). For each of the two cases we apply a perturbation $\gamma_p = 0.25$ Sv for a period of $t_m = 20$ yr and for a period of $t_m = 23$ yr. The time scale can be easily increased by changing the parameters as summarized in Table 1 and is not essential here. Figure 12c shows that the system recovers after both perturbations when $F_1 < 0$, which is in the SE regime. On the other hand, when $F_1 > 0$, the system recovers for $t_m = 20$ yr, but collapses for $t_m = 23$ yr.

The fluxes and salinities may be written as the sum of a mean state (\bar{m} , \bar{S}_i) and a perturbation (\tilde{m} , \tilde{S}_i). Since total salinity is conserved, the evolution of the Atlantic salinity is proportional to $-d\tilde{S}_1/dt$, which for positive m is given by

$$V_1 \frac{d\tilde{S}_1}{dt} = \tilde{m} (\bar{S}_4 - \bar{S}_1) + \bar{m} (\tilde{S}_4 - \tilde{S}_1) + \tilde{m} (\tilde{S}_4 - \tilde{S}_1), \quad (22)$$

which has a similar interpretation as (17) for the global ocean model. The time evolution of these three terms is shown in Fig. 12d for the case $t_m = 23$ yr both for the system residing in the single (red curves) and in the multiple equilibrium regime (blue curves). Similar to the the results in the global ocean model, the term $\bar{m} (\tilde{S}_4 - \tilde{S}_1)$ is stabilizing (it leads to an increase in Atlantic salinity) and the term $\tilde{m} (\tilde{S}_4 - \tilde{S}_1)$ is destabilizing. The two terms $\bar{m} (\tilde{S}_4 - \tilde{S}_1)$ and $\tilde{m} (\tilde{S}_4 - \tilde{S}_1)$ are very similar in both ME and SE regimes.

The change from SE to ME regime is, just as in the global ocean model, also related to a sign change in the term $\tilde{m} (\bar{S}_4 - \bar{S}_1)$. The nice element in the box model is that the steady state salinity contrast is given by

$$\bar{S}_4 - \bar{S}_1 = -\frac{S_0 F_1}{\bar{m}}. \quad (23)$$

and hence its sign is directly coupled to that of F_1 . Since $\bar{m} > 0$ and $\tilde{m} < 0$ in both regimes, the term $\tilde{m} (\bar{S}_4 - \bar{S}_1)$ will switch sign when F_1 (in the box model the equivalent to M_{ov} in the global model) switches sign which is exactly at the boundary between SE and ME regime (Fig. 12b).

5 Summary and Discussion

Using a fully-implicit global ocean model coupled to an energy balance atmosphere model, we revisited the problem of the characterization of the multiple equilibrium (ME) regime of the Atlantic MOC through an indicator Σ given by (1). Our ocean model certainly has many deficiencies (Dijkstra and Weijer, 2005) such that western boundary currents are very broad, the wind-driven gyre flows are relatively weak and eddy processes are completely ignored. The discussion below should be considered with these limitations in mind. The main advantages of the model approach here is that (i) full bifurcation diagrams can be computed versus the freshwater flux parameter γ_p and that (ii) the freshwater balances over the Atlantic basin are accurately satisfied. A detailed connection can therefore be made between the position of the saddle-node bifurcations bounding the hysteresis regime of the Atlantic MOC and changes in the Atlantic freshwater budget.

Our aim was to provide a better physical picture why the indicator Σ has a zero on the ‘on’ branch for the value of γ_{L-} , where we find the saddle-node bifurcation L_- on the ‘off’ branch. This is a nonlinear problem as entering the ME regime from the SE regime when γ_p is increased is related to a change in the development of finite amplitude perturbations. The ‘on’ state is stable to small perturbations in both SE

and ME regime. Our approach was to add controlled perturbations (an anomalous freshwater flux) for a time t_m and then analyze the differences in the evolution of the Atlantic freshwater budget between both ME and SE regimes.

The equation (17) clearly illustrates the importance of the freshwater fluxes at the southern boundary. Interactions between the perturbed flow and the background steady state, as well as nonlinear driven freshwater transport, directly contribute to the tendency of the volume averaged salinity perturbation in the Atlantic basin. At the value of γ_p where the steady state value of $\Sigma \approx M_{ov}(35^\circ\text{S})$ changes sign, also the anomalous salinity transport associated with the $\tilde{v}\bar{S}$ term changes sign. As the steady state meridional velocity \bar{v} does not change much with γ_p on the ‘on’ branch, the sign of Σ is closely coupled to that of the steady state salinity field at 35°S . With increasing γ_p the salinity at depth decreases (there is freshwater export in the ME regime) and hence the $\tilde{v}\bar{S}$ term becomes more destabilizing (again because \tilde{v} is very similar for the SE and ME regime).

This connection between properties of the steady states and the processes controlling the evolution of perturbations was most clearly illustrated with the box model analysis in section 5.3. When the MOC decreases due to change in freshwater flux in the northern box, the interaction of the velocity perturbation and the steady state salinity field transports salt into the Atlantic basin in the SE regime and freshwater in the ME regime. While in the box model the meridional advection terms in the salinity equation are the only relevant process, we have assumed that these terms are dominant in the global ocean model (as reflected in the equation (17)).

Climate models that were integrated as part of the SRESA1B-scenario of the IPCC do not show any sign of abrupt change in the Atlantic MOC (Schmittner *et al.*, 2005), although this does not prove that the models do not have a ME regime. Model intercomparison studies show no systematic differences in THC behavior and climate response between EMICs and AOGCM’s (Gregory *et al.*, 2005; Stouffer

et al., 2006). The ME regime is present in simple coupled models (De Vries and Weber, 2005; Rahmstorf *et al.*, 2005; Weber *et al.*, 2007) and in some more complex coupled models (Manabe and Stouffer, 1988). Atmospheric feedbacks may indeed change the crucial role of the salt-advection feedback by affecting the east-west salinity difference at 35°S in response to a temporarily decrease in the Atlantic MOC. However, when they would completely remove the ME regime, it becomes more difficult to explain the paleoclimatic record (Clark *et al.*, 2002).

Before discussing the applicability of Σ as an indicator of multiple equilibria in GCMs and in observations, we mention explicitly that the model used here has a relatively large vertical diffusivity and hence the MOC is in the ‘mixing’ regime. When K_V is decreased, several cases can be distinguished: (i) the multiple equilibria disappear, (ii) there are still multiple equilibria but because the MOC is more ‘wind-driven’ the quantity Σ would not be a good indicator and (iii) the multiple equilibria remain and Σ is still a good indicator. Support for (iii) is provided by the results in Weber *et al.* (2007) but a detailed study what happens with the bifurcation diagrams when decreasing K_V would require much more work. It would also require a different model, as low vertical diffusivity regimes cannot be reached with the model used in this paper.

Calculating Σ to investigate multistability in coupled GCMs is rather straightforward and has the advantage of inferring the stability regime from the equilibrium solution, without having to perform hosing experiments. When the MOC changes in these models, the freshwater flux field changes in a complicated way, and there are also changes in the wind field and the heat flux field. However, based on the increased knowledge of the physics behind the indicator Σ , we think that it is a relevant diagnostic for the stability properties of the MOC in coupled GCMs as it is related to (intrinsic) advective processes in the Atlantic freshwater budget.

Yin and Stouffer (2007) compared the development of the MOC to freshwater perturbations in two different versions of the GFDL model. They attributed the

different behavior of the MOC in these models to the different character of the ‘off’ states and to different atmospheric feedbacks. However, from their analysis it can be deduced that Σ is negative in the model where the ‘off’ state appears to be stable and is characterized by a reversed MOC. In the other model, Σ is positive and a weakened ‘on’ state is found, that evolves back to the ‘on’ state MOC when the hosing stops, regardless the atmospheric feedbacks. This behavior is consistent with the hypothesis that the sign of Σ determines the regime of the MOC.

It is interesting to see that the result on Σ strongly depends on the depth of the zero contour of the MOC. When the position of the zero contour is at shallower depth, Σ tends to be more negative and hence there is a tendency to the multiple equilibrium regime. This is actually seen in GCMs where the MOC shoals under increasing greenhouse gas concentrations (Stouffer *et al.*, 2006). Also in simulations of glacial climates, there are indications for a shoaling of the MOC (Weber *et al.*, 2007) again pointing to a MOC which is more likely to be in a multiple equilibrium regime.

To address the important question where the real ocean resides, estimates of Σ can be made. Using data from an inversion of WOCE data by Holfort (1994), Weijer *et al.* (1999) concluded that the MOC exports freshwater at 30°S. They determined a present day value of $\Sigma \approx M_{ov}(30^\circ\text{S}) \approx -0.3$ Sv and no error estimate was given. Using a recent data set (Gouretski and Koltermann, 2004), we determined the zonally averaged salinity profile at 35°S (Fig. 13a) and calculated a zonal mean velocity profile based on thermal wind balance with the same method as was used to obtain Fig. 8.2 in Van Aken (2007). An Ekman transport of 4 Sv was added to obtain a zero integral of the section averaged volume transport (as required in steady state); the result is shown in Fig. 13b. From these profiles, we obtain $\Sigma = M_{ov}(35^\circ\text{S}) \approx -0.1$ Sv; an Ekman transport change of 2 Sv gives a difference of 0.02 Sv in Σ . Similar to the results in Weijer *et al.* (1999), this would indicate that the present day MOC is in the ME regime. Obviously, this result probably has a large error bar

as Σ will be a highly fluctuating quantity affected by many processes not considered here (such as the effect of the Bering Strait transport). We hope, however, that this value for Σ and the results in this paper will stimulate analysis of combined data sets from observations and model simulations (such as in Garzoli and Baringer (2007)) to provide better estimates of present day values of Σ .

The main result of this paper is that we provide a physical justification that a negative sign of Σ is a good indicator for the multiple equilibrium regime of the MOC. The results in section 4.2 show that, when a freshwater perturbation is imposed on the ‘on’ state of the MOC, Σ is a measure for the anomalous freshwater transport into/out of the Atlantic induced by velocity perturbations and the background salinity field. This transport is stabilizing the MOC (making the Atlantic saltier) in the SE regime for which the background MOC is exporting salt. However, it is destabilizing (freshening the Atlantic) in case the MOC exports freshwater. The analysis fully supports and corroborates earlier descriptive explanations (Rahmstorf, 1996; De Vries and Weber, 2005; Dijkstra, 2007) and provides the details of the processes involved.

Acknowledgements

Computations were done on the Huygens IBM p6 supercomputer at SARA Amsterdam. Use of these computing facilities was sponsored by the National Computing Facilities Foundation (N.C.F.) under the project SH084-08 with financial support from the Netherlands Organization for Scientific Research (N.W.O.). This work was supported by a NWO Toptalent Grant to one of the authors (MdT). We thank both Stefan Rahmstorf and another anonymous referee for very useful comments on the first version of this paper.

References

- Clark, P. U., Pisias, N. G., Stocker, T. F., and Weaver, A. J. (2002). The role of the thermohaline circulation in abrupt climate change. *Nature*, **415**, 863–869.
- De Vries, P. and Weber, S. L. (2005). The Atlantic freshwater budget as a diagnostic for the existence of a stable shut down of the meridional overturning circulation. *Geophys. Res. Letters*, **32**, No.9,L09606.
- Dijkstra, H. A. (2007). Characterization of the multiple equilibria regime in a global ocean model. *Tellus*, **59A**, 695–705.
- Dijkstra, H. A. and Molemaker, M. J. (1997). Symmetry breaking and overturning oscillations in thermohaline-driven flows. *J. Fluid Mech.*, **331**, 195–232.
- Dijkstra, H. A. and Weijer, W. (2005). Stability of the global ocean circulation: basic bifurcation diagrams. *J. Phys. Oceanogr.*, **35**, 933–948.
- Dijkstra, H. A., Te Raa, L. A., and Weijer, W. (2004). A systematic approach to determine thresholds of the ocean’s thermohaline circulation. *Tellus*, **56A**, 362–370.
- Garzoli, S. and Baringer, M. O. (2007). Meridional heat transport determined with expendable bathythermographs. Part II: South Atlantic transport. *Deep-Sea Research*, **54**, 1402–1420.
- Gouretski, V. V. and Koltermann, K. P. (2004). Berichte des Bundesambtes für Seeschiffahrt und Hydrographie. Technical Report 35, .
- Gregory, J. M., Dixon, K. W., Stouffer, R. J., Weaver, A. J., Driesschaert, E., Eby, M., Fichefet, T., Hasumi, H., Hu, A., Jungclaus, J. H., Kamenkovich, I. V., Levermann, A., Montoya, M., Murakami, S., Nawrath, S., Oka, A., Sokolov, A. P., and Thorpe, R. B. (2005). A model intercomparison of changes in the Atlantic

- thermohaline circulation in response to increasing atmospheric CO_2 concentration. *Geophys. Res. Letters*, **32**, 12703–+.
- Holfort, J. (1994). *Grossräumige Zirkulation und meridionale transporte in Südatlantik*. Ph.D. thesis, Institut für Meereskunde, Kiel, Germany.
- Kuhlbrodt, T., Griesel, A., Montoya, M., Levermann, A., and Rahmstorf, S. (2007). On the driving processes of the atlantic meridional overturning circulation On the Driving Processes of the Atlantic Meridional Overturning Circulation. *Reviews of Geophysics*, **45**.
- Levitus, S. (1994). World Ocean Atlas 1994, Volume 4: Temperature. *NOAA/NESDIS E, US Department of Commerce, Washington DC*, **OC21**, 1–117.
- Manabe, S. and Stouffer, R. J. (1988). Two stable equilibria of a coupled ocean-atmosphere model. *J. Climate*, **1**, 841–866.
- Rahmstorf, S. (1996). On the freshwater forcing and transport of the Atlantic thermohaline circulation. *Clim. Dyn.*, **12**, 799–811.
- Rahmstorf, S. (2002). Ocean circulation and climate changes during the past 120,000 years. *Nature*, **419**, 207–214.
- Rahmstorf, S. (2003). The current climate. *Nature*, **421**, 699.
- Rahmstorf, S., Crucifix, M., Ganopolski, A., Goosse, H., Kamenkovich, I., Knutti, R., Lohmann, G., March, R., Mysak, L., Wang, Z., and Weaver, A. J. (2005). Thermohaline circulation hysteresis: a model intercomparison. *Geophys. Res. Letters*, **L23605**, doi:0.1029/2005GLO23655, 1–5.
- Schmittner, A., Latif, M., and Schneider, B. (2005). Model projections of the North

- Atlantic thermohaline circulation for the 21st century assessed by observations. *Geophys. Res. Letters*, **L23710**, doi:10.1029/2005GLO24368, 1–4.
- Stommel, H. (1961). Thermohaline convection with two stable regimes of flow. *Tellus*, **2**, 244–230.
- Stouffer, R. J., Yin, J., Gregory, J. M., Dixon, K. W., Spelman, M. J., Hurlin, W., Weaver, A. J., Eby, M., Flato, G. M., Hasumi, H., Hu, A., Jungclaus, J., Kamenkovich, I. V., Levermann, A., Montoya, M., Murakami, S., Nawrath, S., Oka, A., Peltier, W. R., Robitaille, D. Y., Sokolov, A., Vettoretti, G., and Weber, S. L. (2006). Investigating the Causes of the Response of the Thermohaline Circulation to Past and Future Climate Changes. *J. Climate*, **19**, 1365–1387.
- Trenberth, K. E., Olson, J. G., and Large, W. G. (1989). A global ocean wind stress climatology based on ECMWF analyses. Technical report, National Center for Atmospheric Research, Boulder, CO, U.S.A.
- Van Aken, H. M. (2007). *The Oceanic Thermohaline Circulation*. Springer.
- Vellinga, M., Wood, R. A., and Gregory, J. M. (2002). Processes governing the recovery of a perturbed thermohaline circulation in HadCM3. *J. Climate*, **15**, 764–780.
- Walsh, G. (1985). The thermohaline circulation and the control of ice ages. *Paleogeogr. Paleoclim. Paleoecol.*, **50**, 323–332.
- Weber, S. L., Drijfhout, S. S., Abe-Ouchi, A., Crucifix, M., Eby, M., Ganopolski, A., Murakami, S., Otto-Bliesner, B., and Peltier, W. R. (2007). The modern and glacial overturning circulation in the Atlantic ocean in PMIP coupled model simulations. *Climate of the Past*, **3**, 51–64.
- Weijer, W., De Ruijter, W. P. M., Dijkstra, H. A., and Van Leeuwen, P. J. (1999).

Impact of interbasin exchange on the Atlantic overturning circulation. *J. Phys. Oceanogr.*, **29**, 2266–2284.

Wunsch, C. (2002). What is the thermohaline circulation? *Science*, **298**, 1179–1180.

Yin, J. and Stouffer, R. J. (2007). Comparison of the Stability of the Atlantic Thermohaline Circulation in Two Coupled Atmosphere-Ocean General Circulation Models. *J. Climate*, **20**, 4293–4315.

Table Captions

1. Values of parameters used in the numerical calculations for the box model.

Figure Captions

1. (a) Bifurcation diagram where the strength of the Atlantic MOC (ψ_A) is plotted versus the strength of the anomalous freshwater forcing (γ_p). The labeling [a]-[f] along the branches refers to steady-state solutions of which the meridional overturning is plotted in Fig. 2. (b) Indicator function $\Sigma(\theta_s, \theta_n)$ for $\theta_n = 60^\circ\text{N}$ and $\theta_s = 35^\circ\text{S}$ along the ‘on’ branch of the bifurcation diagram in (a). The vertical dotted lines indicate the positions of L_- and L_+ .

2. Contour plots of the Atlantic MOC for several values of γ_p along curve in Fig. 1. Contour values are in Sv. (a) $\gamma_p = 0.042$ Sv, $\psi_A = 13.50$ Sv. (b) $\gamma_p = 0.125$ Sv, $\psi_A = 11.87$ Sv. (c) $\gamma_p = 0.234$ Sv, $\psi_A = 7.32$ Sv. (d) $\gamma_p = 0.121$ Sv, $\psi_A = 4.90$ Sv. (e) $\gamma_p = 0.170$ Sv, $\psi_A = 4.44$ Sv. (f) $\gamma_p = 0.393$ Sv, $\psi_A = 3.63$ Sv.

3. All terms in the freshwater balance (10) along the bifurcation diagram in Fig. 1. (a) Southern boundary $\theta_s = 35^\circ\text{S}$ and (b) Northern boundary $\theta_n = 60^\circ\text{N}$ of the Atlantic.

4. (a) $M_{az}(\theta)$ as a function of latitude θ for the solutions Fig. 2a-c on the ‘off’ branch. (b) $M_{ov}(\theta)$ as a function of latitude θ for the solutions Fig. 2a-c on the ‘off’ branch.

5. (a) $M_{az}(\theta)$ as a function of latitude θ for the solutions Fig. 2a-c on the ‘on’ branch. (b) $M_{ov}(\theta)$ as a function of latitude θ for the solutions Fig. 2a-c on the ‘on’ branch.

6. Contour plots of the meridional velocity \bar{v} (a, c) and salinity \bar{S} (b, d) field along the Atlantic 35°S section for both the steady state (a,b) in the SE regime ($\bar{\gamma}_p^S = 0.083$ Sv) and the one (c,d) in the ME regime ($\bar{\gamma}_p^M = 0.166$ Sv).

7. Strength (ψ_A) in Sv of the Atlantic MOC along trajectories (drawn) for a permanent freshwater flux change for both the SE (red) regime ($\bar{\gamma}_p^S = 0.083$ Sv) and the ME (blue) regime ($\bar{\gamma}_p^M = 0.166$ Sv). The dashed are trajectories for which the freshwater flux change is reduced to zero at certain times t_m ; the latter time can be deduced from the starting point of each dashed curve. (a) A very small change, $\Delta\gamma_p^S = \Delta\gamma_p^M = 0.02$ Sv. (b) A larger change, $\Delta\gamma_p^S = 0.197$ Sv and $\Delta\gamma_p^M = 0.114$ Sv.

8. (a) Time development of the three different terms in the right hand side of (17) along the drawn trajectories in Fig. 7a. The color coding corresponds to that in Fig. 7a (red: SE regime; blue: ME regime) and a similar line style indicates a similar term. (b) Integral terms in (18). The dotted curve is again the $\tilde{v}\bar{S}$ integral term similar to the one in (a). The drawn (dashed-dotted) curve is the first (second) term in the right hand side of (18).

9. Contour plots of the meridional velocity (a, c) and salinity (b, d) perturbations at year 200 field along the Atlantic 35°S section for both the SE regime ($\bar{\gamma}_p^S = 0.083$ Sv) and the ME regime ($\bar{\gamma}_p^M = 0.166$ Sv) under the change $\Delta\gamma_p^S = \Delta\gamma_p^M = 0.02$ Sv.

10. The field $\tilde{v}\bar{S}$ for (a) the SE regime, (b) the ME regime and their (c) difference. The fields are for the solutions at year 200 (drawn curves) in Fig. 7a.

11. (a) The field $\langle\bar{v}\rangle$ for the steady state at $\bar{\gamma}_p^S = 0.083$ Sv (red) and $\bar{\gamma}_p^M = 0.166$ Sv (blue). (b-c) The fields $\langle\tilde{v}\rangle$ at different times (every 25 year up to year 200) for the ME regime (b) and the SE regime (c). These fields are computed for the solutions

along the drawn curves in Fig. 7a.

12. (a) Simple box model of the Atlantic overturning circulation (Rahmstorf, 1996). Deep convection takes place in box 2. The strength of the cross equatorial flow is controlled by the density contrast between boxes 2 and 1. The temperatures T_1 and T_2 are prescribed, while salinities are determined by the flow and the ‘active’ freshwater fluxes F_1 and F_2 . (b) Bifurcation diagram showing the steady solutions with positive transport versus F_1 . (c) Overturning strength m as function of time for the four perturbation experiments. (d) Negative time rate of change of the salinity in box 1 as function of time, split into the three contributions given in equation (22). Term 1 corresponds to $\tilde{m}(\bar{S}_4 - \bar{S}_1)$, term 2 to $\bar{m}(\tilde{S}_4 - \tilde{S}_1)$ and term 3 to $\tilde{m}(\tilde{S}_4 - \tilde{S}_1)$.

13. (a) Zonally averaged salinity field from the dataset in Gouretski and Koltermann (2004). (b) Zonally averaged meridional velocity field as determined from the same dataset.

k	$=$	2.7×10^4	Sv	S_0	$=$	35.0	psu	V_1	$=$	4.0×10^{16}	m^3
α	$=$	1.0×10^{-4}	K^{-1}	F_2	$=$	1.0×10^{-2}	Sv	V_2	$=$	1.0×10^{16}	m^3
β	$=$	7.6×10^{-4}	[]	A_1	$=$	1.0×10^{13}	m^2	V_3	$=$	1.0×10^{17}	m^3
$T_1 - T_2$	$=$	4.5	K	A_3	$=$	1.0×10^{14}	m^2	V_4	$=$	2.0×10^{17}	m^3

Table 1: Values of parameters used in the numerical calculations for the box model.

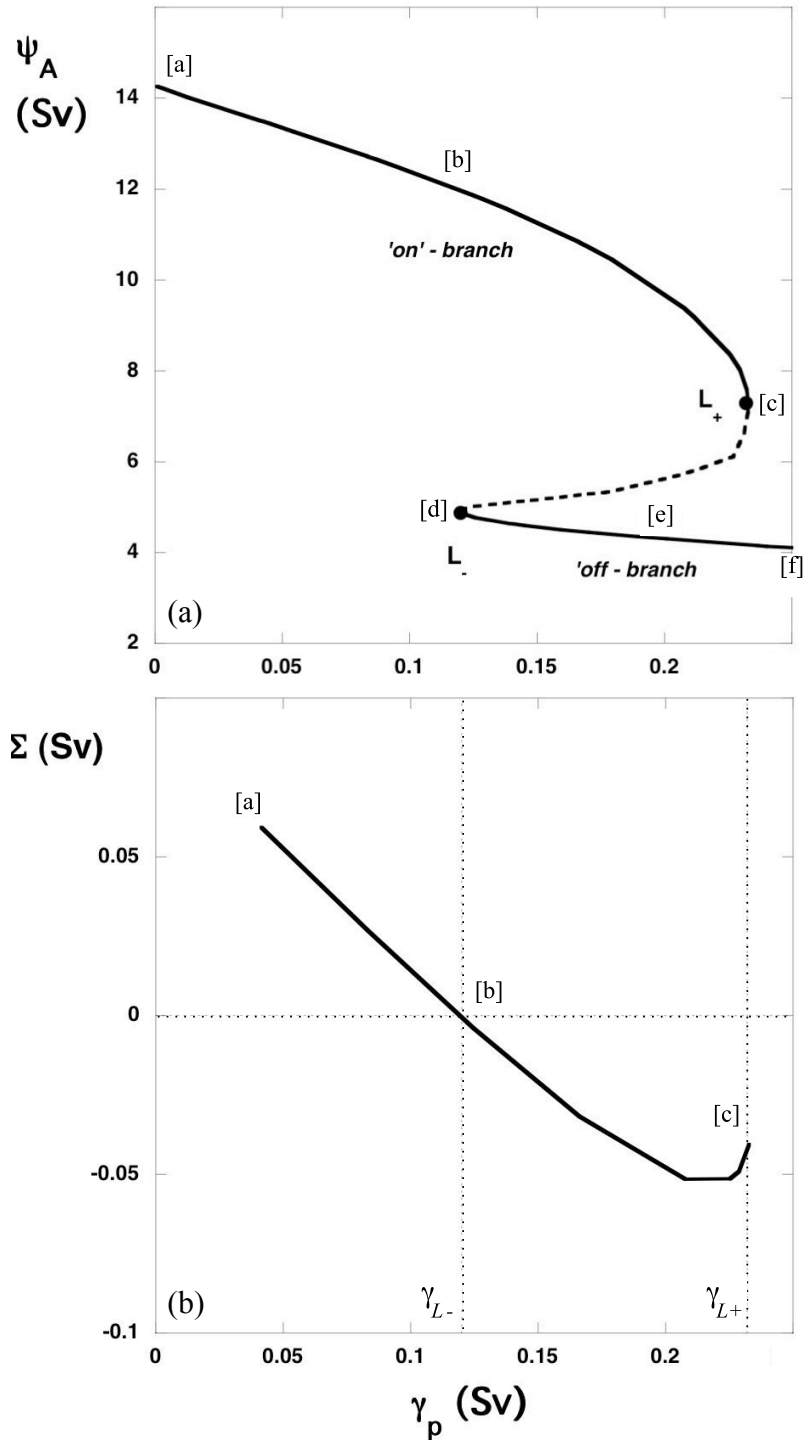


Figure 1: (a) Bifurcation diagram where the strength of the Atlantic MOC (ψ_A) is plotted versus the strength of the anomalous freshwater forcing (γ_p). The labeling [a]-[f] along the branches refers to steady-state solutions of which the meridional overturning is plotted in Fig. 2. (b) Indicator function $\Sigma(\theta_s, \theta_n)$ for $\theta_n = 60^\circ N$ and $\theta_s = 35^\circ S$ along the 'on' branch of the bifurcation diagram in (a). The vertical dotted lines indicate the positions of L_- and L_+ .

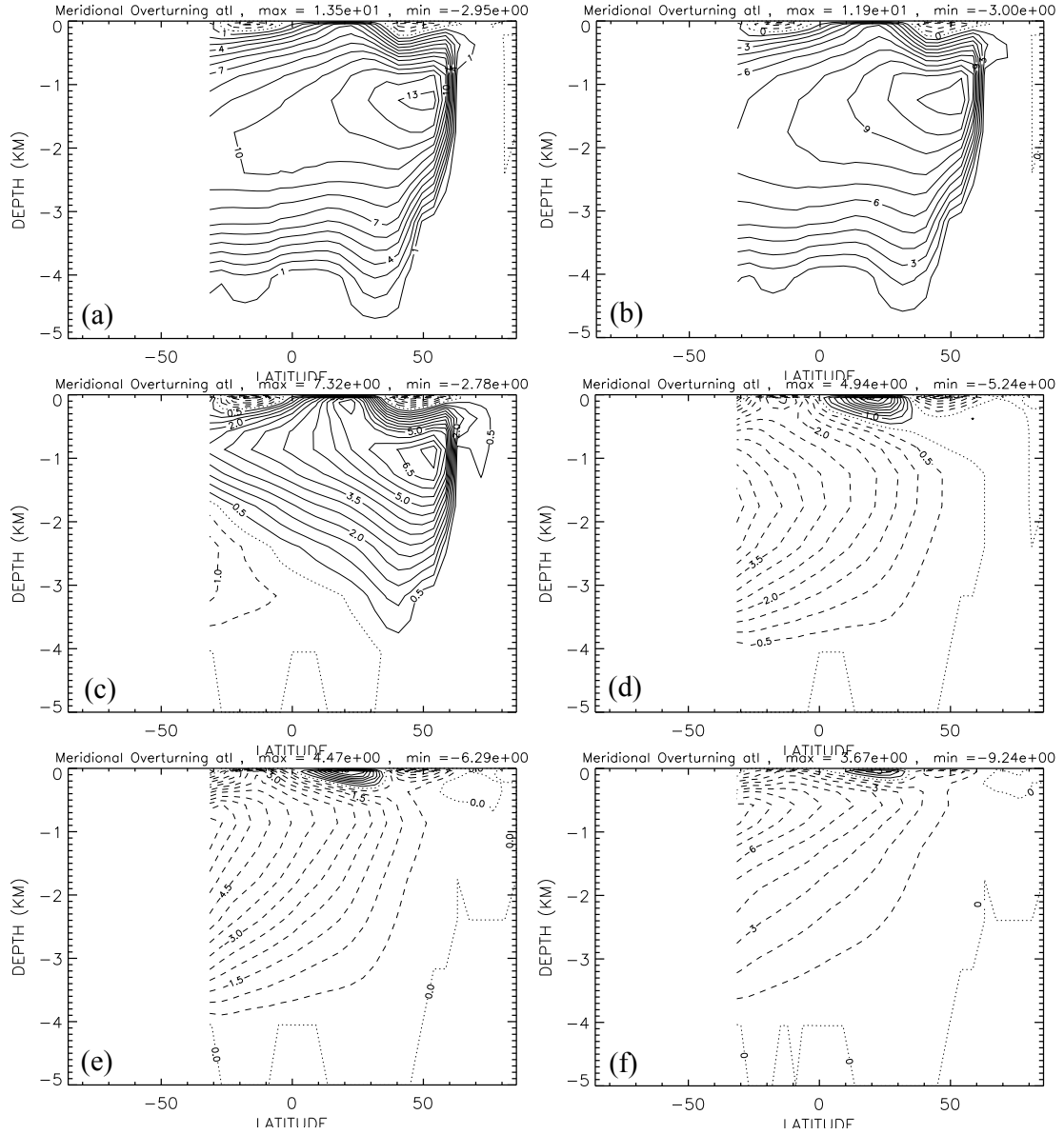


Figure 2: Contour plots of the Atlantic MOC for several values of γ_p along the curve in Fig. 1. Contour values are in Sv. (a) $\gamma_p = 0.042$ Sv, $\psi_A = 13.50$ Sv. (b) $\gamma_p = 0.125$ Sv, $\psi_A = 11.87$ Sv. (c) $\gamma_p = 0.234$ Sv, $\psi_A = 7.32$ Sv. (d) $\gamma_p = 0.121$ Sv, $\psi_A = 4.90$ Sv. (e) $\gamma_p = 0.170$ Sv, $\psi_A = 4.44$ Sv. (f) $\gamma_p = 0.393$ Sv, $\psi_A = 3.63$ Sv.

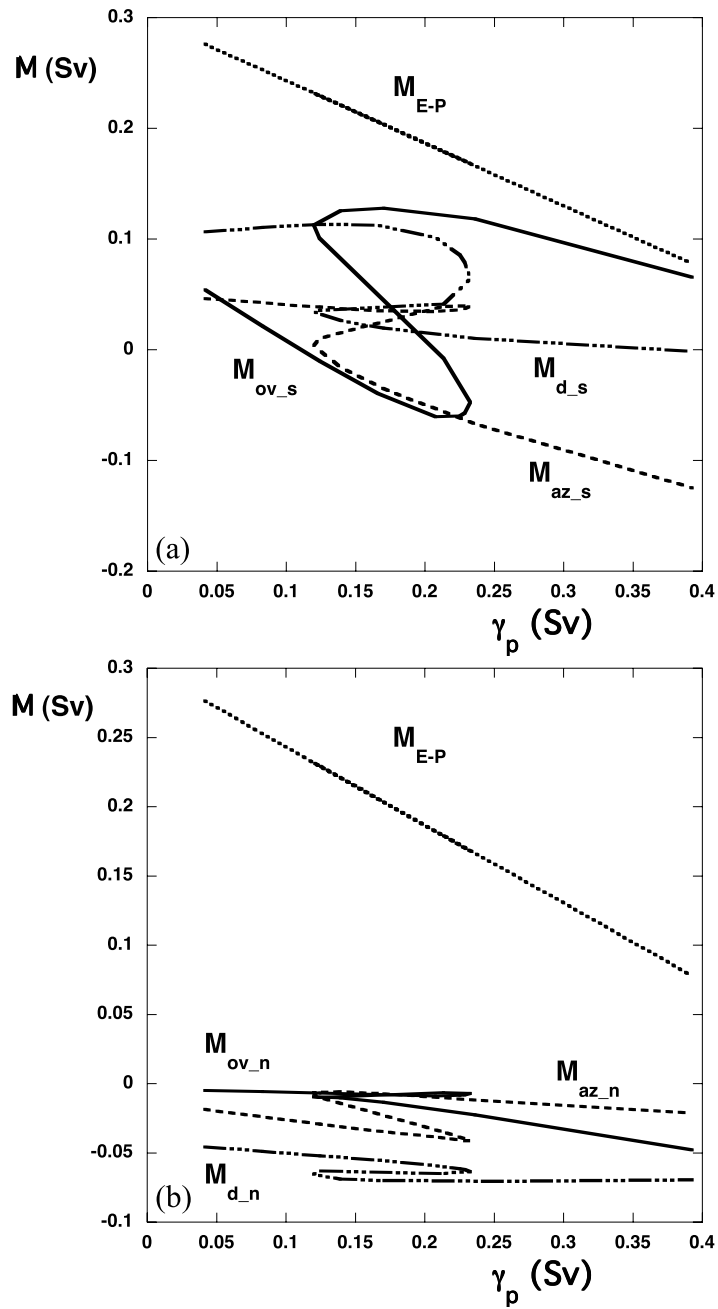


Figure 3: All terms in the freshwater balance (10) along the bifurcation diagram in Fig. 1. (a) Southern boundary $\theta_s = 35^\circ\text{S}$ and (b) Northern boundary $\theta_n = 60^\circ\text{N}$ of the Atlantic.

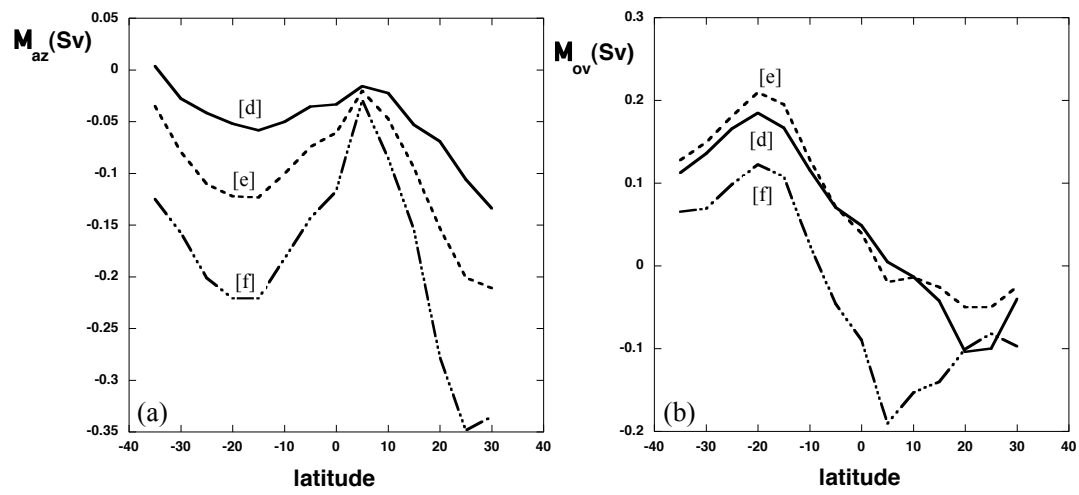


Figure 4: (a) $M_{az}(\theta)$ as a function of latitude θ for the solutions in Fig. 2d-f on the ‘off’ branch. (b) $M_{ov}(\theta)$ as a function of latitude θ for the solutions in Fig. 2d-f on the ‘off’ branch.

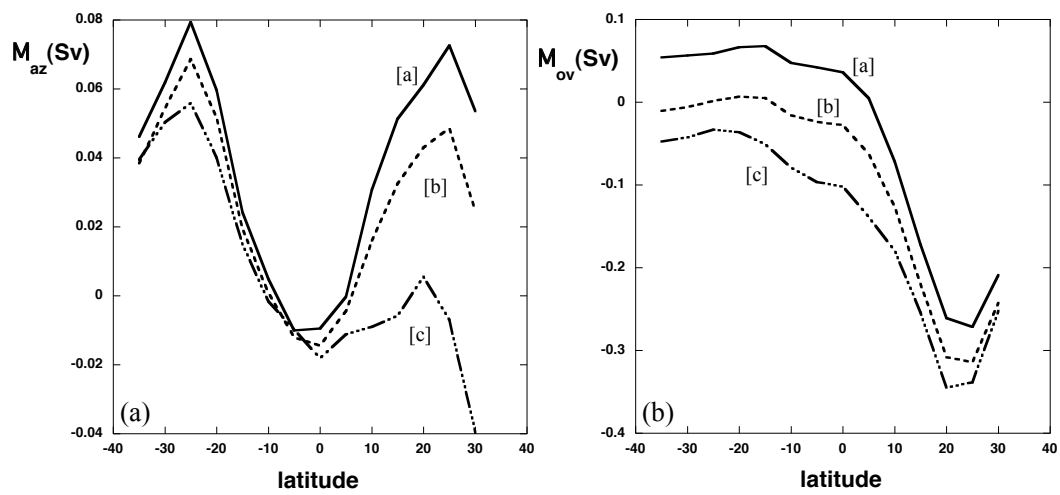


Figure 5: (a) $M_{az}(\theta)$ as a function of latitude θ for the solutions Fig. 2a-c on the ‘on’ branch. (b) $M_{ov}(\theta)$ as a function of latitude θ for the solutions Fig. 2a-c on the ‘on’ branch.

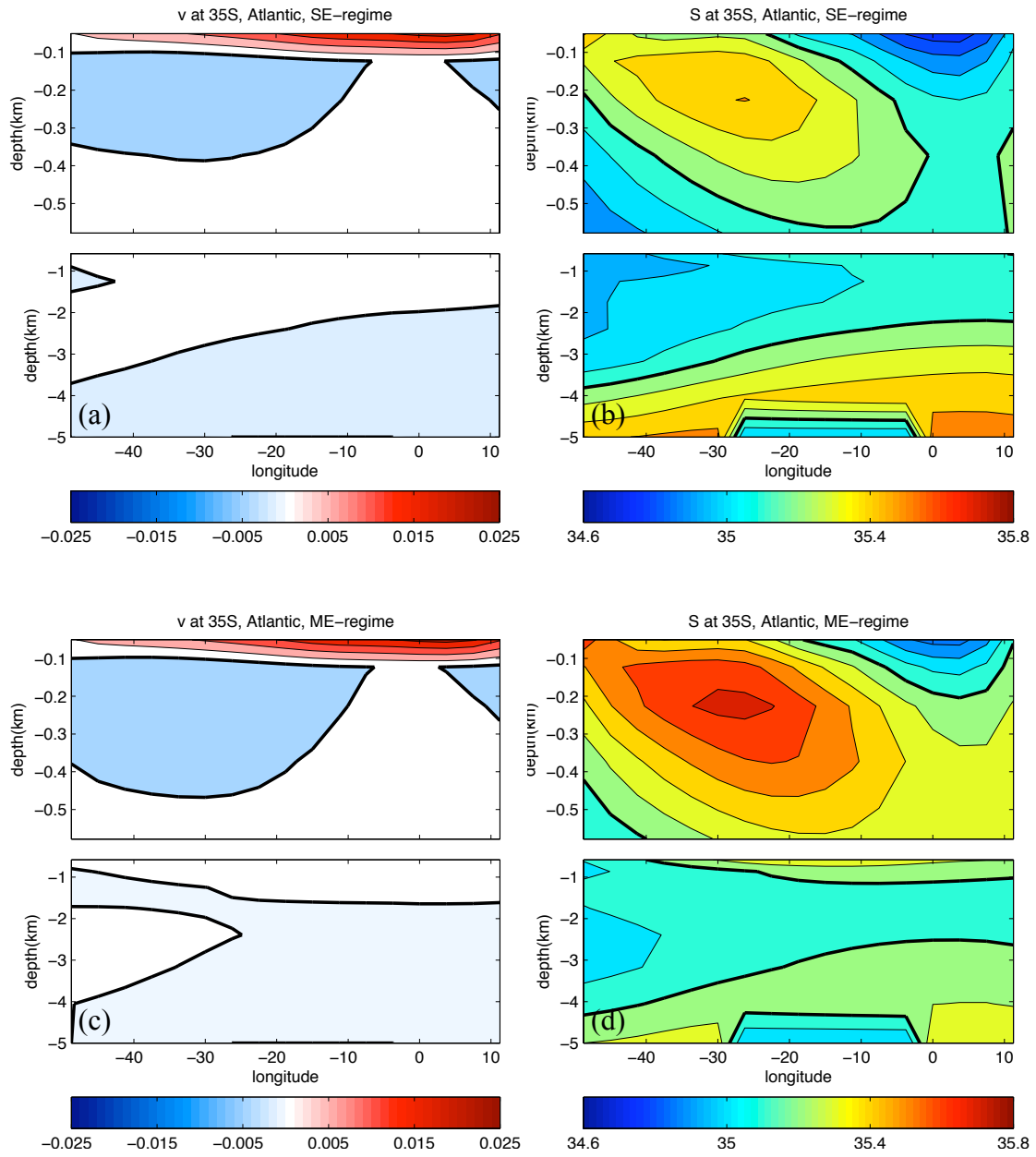


Figure 6: Contour plots of the meridional velocity \bar{v} (a, c) and salinity \bar{S} (b, d) field along the Atlantic 35°S section for both the steady state (a,b) in the SE regime ($\bar{\gamma}_p^S = 0.083$ Sv) and the one (c,d) in the ME regime ($\bar{\gamma}_p^M = 0.166$ Sv).

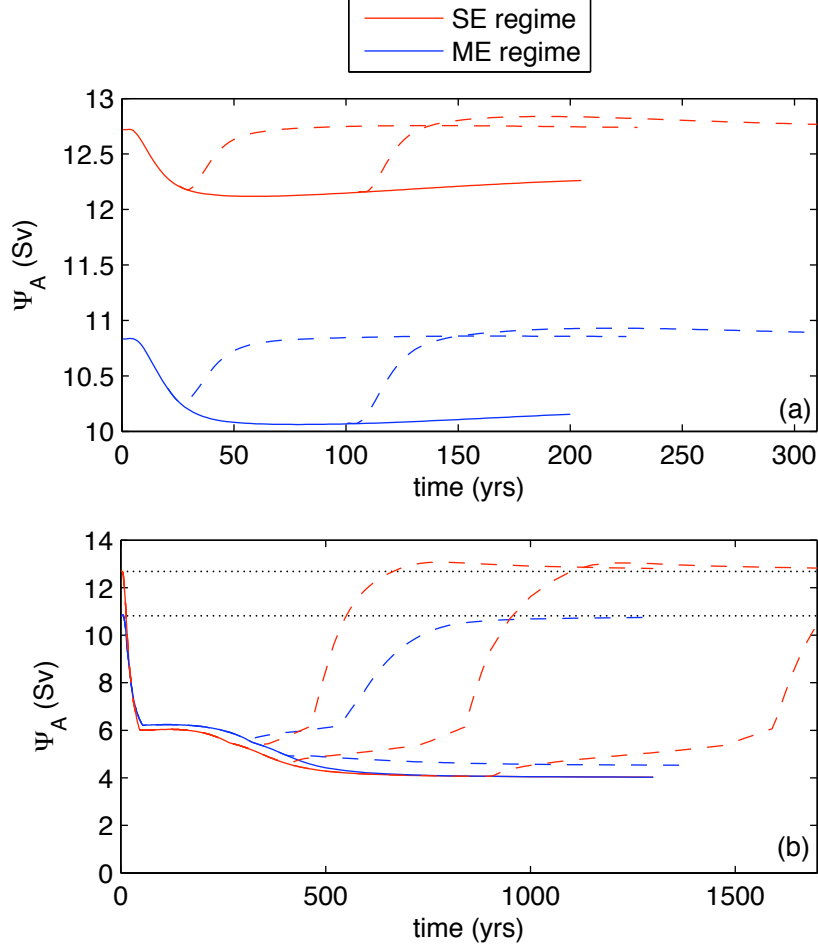


Figure 7: Strength (ψ_A) in Sv of the Atlantic MOC along trajectories (drawn) for a permanent freshwater flux change for both the SE (red) regime ($\bar{\gamma}_p^S = 0.083$ Sv) and the ME (blue) regime ($\bar{\gamma}_p^M = 0.166$ Sv). The dashed are trajectories for which the freshwater flux change is reduced to zero at certain times t_m ; the latter time can be deduced from the starting point of each dashed curve. (a) A very small change, $\Delta\gamma_p^S = \Delta\gamma_p^M = 0.02$ Sv. (b) A larger change, $\Delta\gamma_p^S = 0.197$ Sv and $\Delta\gamma_p^M = 0.114$ Sv.

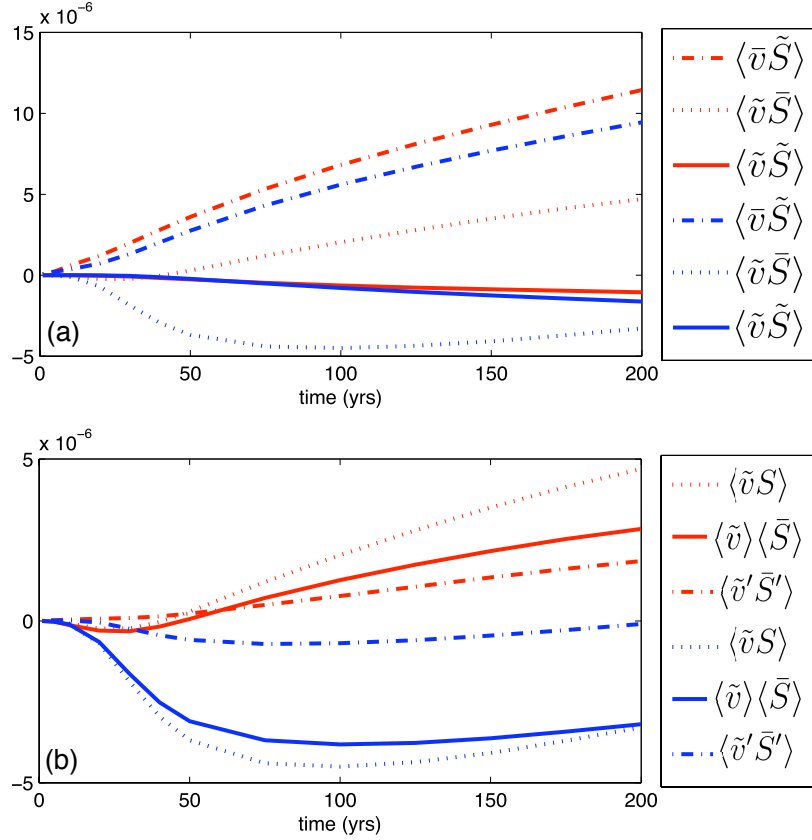


Figure 8: (a) Time development of the three different terms in the right hand side of (17) along the drawn trajectories in Fig. 7a. The color coding corresponds to that in Fig. 7a (red: SE regime; blue: ME regime) and a similar line style indicates a similar term. (b) Integral terms in (18). The dotted curve is again the $\tilde{v}\bar{S}$ integral term similar to the one in (a). The drawn (dashed-dotted) curve is the first (second) term in the right hand side of (18).

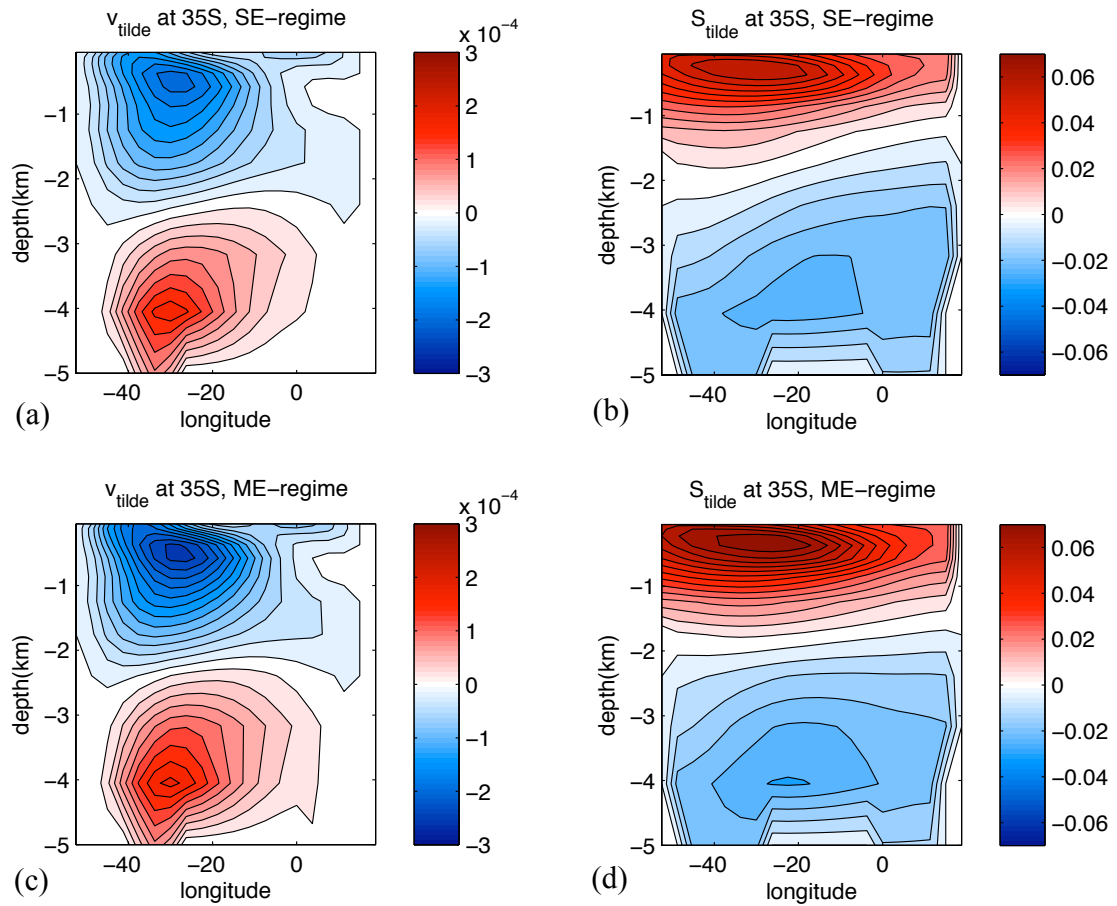


Figure 9: Contour plots of the meridional velocity (a, c) and salinity (b, d) perturbations at year 200 field along the Atlantic 35°S section for both the SE regime ($\bar{\gamma}_p^S = 0.083$ Sv) and the ME regime ($\bar{\gamma}_p^M = 0.166$ Sv) under the change $\Delta\gamma_p^S = \Delta\gamma_p^M = 0.02$ Sv.

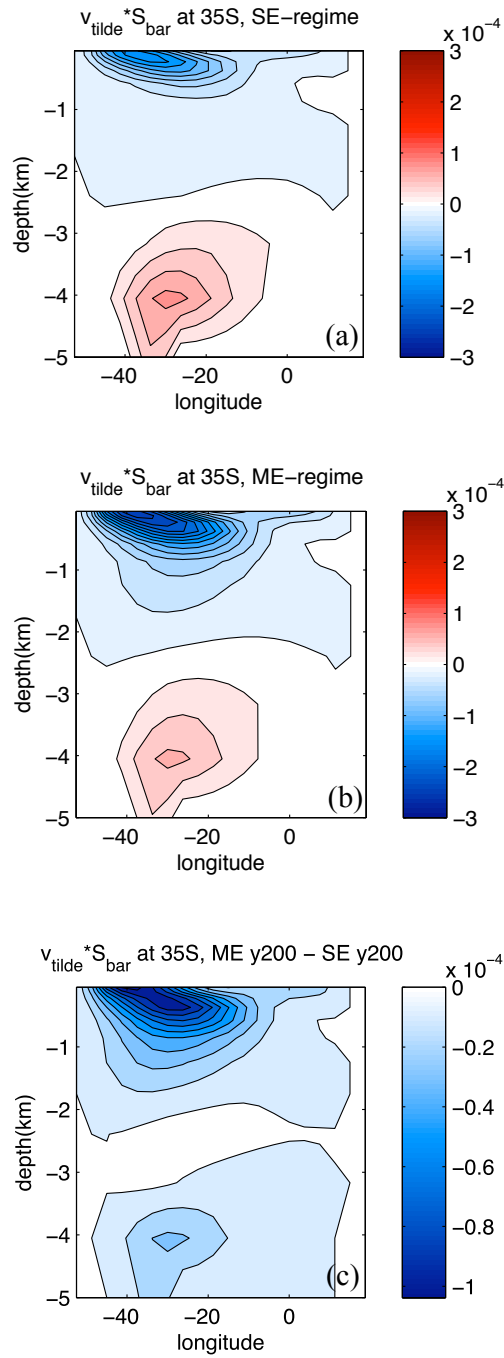


Figure 10: The field $\tilde{v} \bar{S}$ for (a) the SE, (b) the ME regime and their (c) difference. The fields are for the solutions at year 200 (drawn curves) in Fig. 7a.

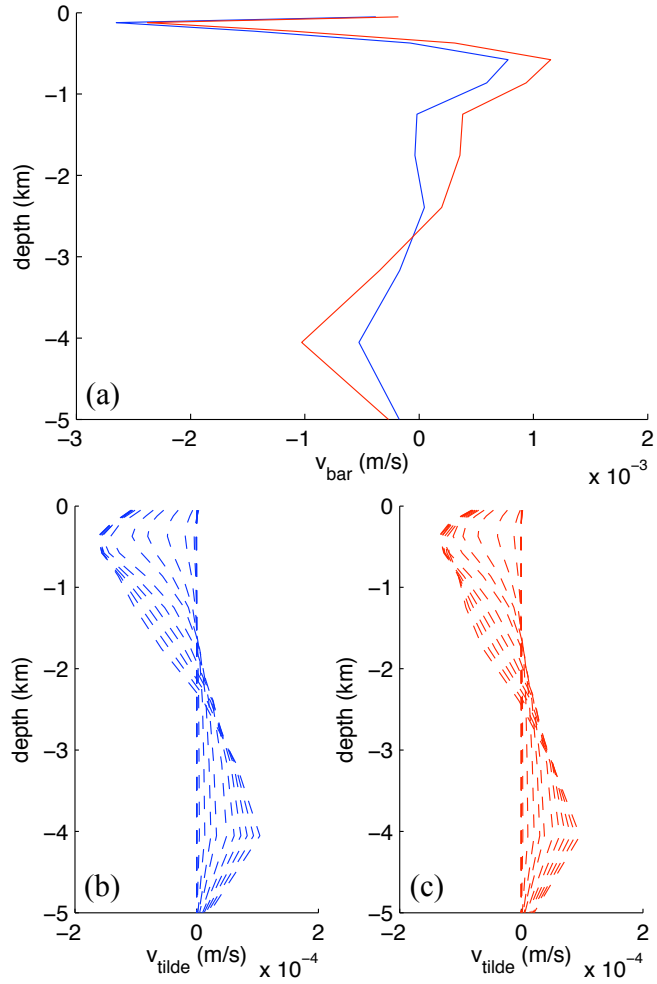


Figure 11: (a) The field $\langle \bar{v} \rangle$ for the steady state at $\bar{\gamma}_p^S = 0.083$ Sv (red) and $\bar{\gamma}_p^M = 0.166$ Sv (blue). (b-c) The fields $\langle \tilde{v} \rangle$ at different times (every 25 year up to year 200) for the ME regime (b) and the SE regime (c). These fields are computed for the solutions along the drawn curves in Fig. 7a.

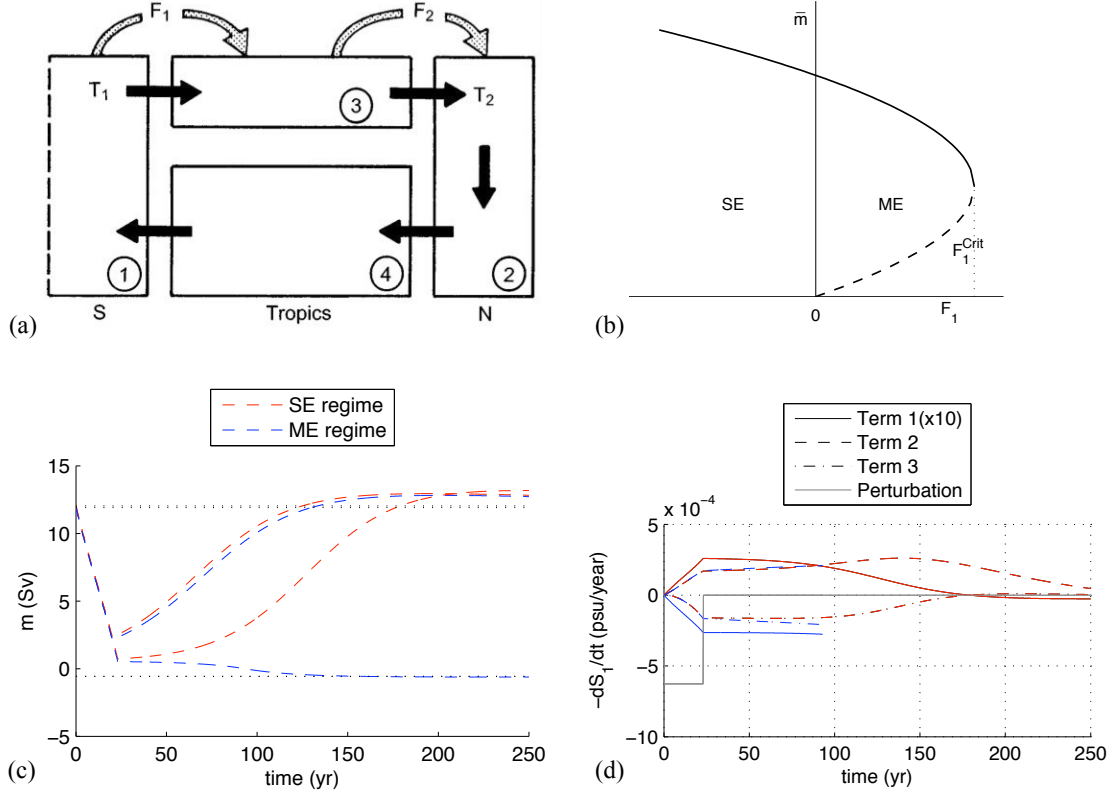


Figure 12: (a) Simple box model of the Atlantic overturning circulation (Rahmstorf, 1996). Deep convection takes place in box 2. The strength of the cross equatorial flow is controlled by the density contrast between boxes 2 and 1. The temperatures T_1 and T_2 are prescribed, while salinities are determined by the flow and the ‘active’ freshwater fluxes F_1 and F_2 . (b) Bifurcation diagram showing the steady solutions with positive transport versus F_1 . (c) Overturning strength m as function of time for the four perturbation experiments. (d) Negative time rate of change of the salinity in box 1 as function of time, split into the three contributions given in equation (22). Term 1 corresponds to $\tilde{m} (\bar{S}_4 - \bar{S}_1)$, term 2 to $\bar{m} (\tilde{S}_4 - \tilde{S}_1)$ and term 3 to $\tilde{m} (\tilde{S}_4 - \tilde{S}_1)$.

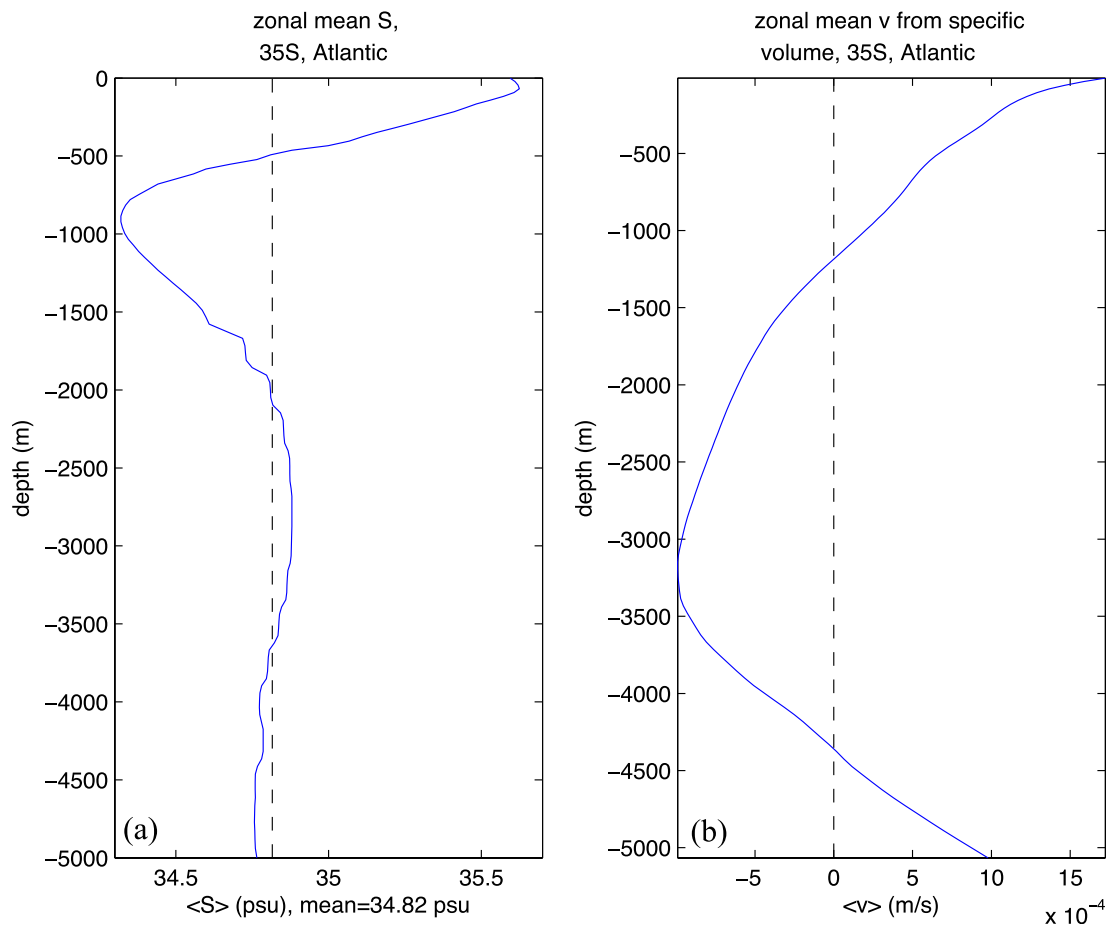


Figure 13: (a) Zonally averaged salinity field from the dataset in Gouretski and Koltermann (2004). (b) Zonally averaged meridional velocity field as determined from the same dataset.